

Quasiparticle Band Gaps, Excitonic Effects, and Anisotropic Optical Properties of Monolayer Distorted 1-T Diamond-Chain Structure ReS_2 and ReSe_2

Hong-Xia Zhong,^{1,2} Shiyuan Gao,¹ Jun-Jie Shi,² and Li Yang¹

¹*Department of Physics, Washington University
in St. Louis, St. Louis, Missouri, 63130, USA*

²*State Key Laboratory for Mesoscopic Physics and Department of Physics,
Peking University, Beijing 100871, China*

Abstract

We report many-body perturbation theory calculations of excited-state properties of distorted 1-T diamond-chain monolayer rhenium disulfide (ReS_2) and diselenide (ReSe_2). Electronic self-energy substantially enhances their quasiparticle band gaps and, surprisingly, converts monolayer ReSe_2 to a direct-gap semiconductor, which was, however, regarded to be an indirect one by density-functional-theory calculations. Their optical absorption spectra are dictated by strongly bound excitons. Unlike hexagonal structures, the lowest-energy bright exciton of distorted 1-T ReS_2 exhibits a perfect figure-8 shape polarization dependence but those of ReSe_2 only exhibit a partial polarization dependence, which results from two nearly-degenerated bright excitons whose polarization preferences are not aligned. Our first-principles calculations are in excellent agreement with experiments and pave the way for optoelectronic applications.

PACS numbers: 71.35.-y, 31.15.A-, 73.22.-f, 78.67.-n

I. INTRODUCTION

To overcome the zero band gap of graphene¹, two-dimensional (2D) transition-metal dichalcogenides (TMDCs) semiconductors have attracted significant attention²⁻⁶. Thanks to the very thin atomic thickness (a few Å), pristine interfaces without out-of-plane dangling bonds, and considerable band gaps (1-2 eV)^{2,7-10}, TMDCs are potentially beneficial for eliminating short channel effects¹¹, lowering interface state densities, reducing surface roughness scattering¹², and low-power digital applications¹³⁻¹⁶. However, because of interlayer interactions and variations of screening, the electronic structures of many hexagonal TMDCs undergo substantial variations with different stacking layer numbers. For example, a crossover from direct band gaps in monolayers to indirect band gaps in multilayers has been observed in MoS₂^{3,4,17}, limiting the applicability of TMDCs in optoelectronic devices.

Layered crystals of rhenium disulfide (ReS₂) and diselenide (ReSe₂) are a new family of 2D TMDCs semiconductors, which have been successfully fabricated recently¹⁸⁻²⁰. Unlike hexagonal TMDCs, ReX₂ (X= S, Se) crystallizes in a distorted 1-T diamond-chain structure with the triclinic symmetry, as a result of charge decoupling from an extra valence electron of Re atoms¹⁸⁻²⁰. This structural distortion leads to a much weaker interlayer coupling. Consequently, the band renormalization is absent and bulk ReX₂ behaves as electronically and vibrationally decoupled monolayers^{18,19}. Such a vanishing interlayer coupling in ReX₂ structures enables probing 2D-like systems without the need of monolayer or few layers, overcoming the challenge of preparing large-area, single-crystal monolayers¹⁸. Furthermore, the structure distortion of 1T-ReX₂ makes it exhibit unique anisotropic optical, electrical, and mechanical properties^{18,20}, with considerable interests for various applications in polarization controller, liquid crystal displays, 3D visualization techniques, (bio)dermatology, and in optical quantum computers^{21,22}.

Despite these unique properties and potential applications of distorted 1-T diamond-chain ReX₂ structures, we have very limited knowledge about their fundamental excited-state properties, such as quasiparticle band gaps, optical spectra, and excitonic effects. In particular, currently available experimental measurements are diverse due to sample qualities and unavoidable environment effects. In this sense, a reliable and parameter-free calculation to accurately capture essential electron-electron (e - e) and electron-hole (e - h) interactions in excited-state properties is highly desirable for understanding fundamental physics and

motivating applications of few-layer ReX_2 .

In this work, we employ the first-principles GW-Bethe-Salpeter Equation (BSE) approach to study two typical distorted 1-T diamond-chain TMDCs, i.e., monolayer ReS_2 and ReSe_2 . We observe significant many-electron effects that dictate their excited-state properties. Self-energy corrections not only enlarge band gaps but also convert suspended monolayer ReSe_2 to be a direct-gap semiconductor. Excitonic effects are prominent and the BSE-calculated absorption spectra are in excellent agreement with measurements. In particular, because of the reduced triclinic symmetry, monolayer ReS_2 and ReSe_2 possess anisotropic optical responses within the near-infrared frequency regime. These excited-state properties within the interesting frequency regime may be useful for optoelectronic applications.

The remainder of this paper is organized as follows: In Sec. II, we introduce the atomic structures of monolayer ReS_2 and ReSe_2 , and our computational approaches. In Sec. III, the quasiparticle band energies, band gaps, and the transition from indirect to a direct band gap, are presented. In Sec. IV, we discuss the optical absorption spectra and excitonic effects. In Sec. V, we focus on the anisotropic optical responses of excitons. In Sec. VI, we summarize our studies and conclusion.

II. ATOMIC STRUCTURE AND COMPUTATIONAL METHODS

The ball-stick structures of monolayer distorted 1-T diamond-chain ReS_2 and ReSe_2 are presented in Fig. 1. The unit cell and unit vectors are marked by purple-colored vectors. Each Re atom is clustering of “diamond chains” composed of the zigzag shape along the \mathbf{a} direction as shown by red-colored lines in Fig. 1(a)^{18,23–25}. The side view of monolayer ReS_2 or ReSe_2 is presented in Fig. 1(b). The special feature is that, unlike hexagonal TMDCs, the S or Se atoms of distorted 1-T diamond-chain structures are not all in the same plane, substantially lowering the structure symmetry. The first Brillouin zone (BZ) is plotted in Fig. 1(c), which is a hexagon but with unequal side lengths as a result of the distorted atomic structure. Consequently, the K1, K2, and K3 points are no longer equivalent.

We fully relax the structures according to the force and stress calculated by DFT with the Perdew, Burke, and Ernzerhof (PBE) functional³⁰, using the QUANTUM ESPRESSO package³¹. The ground-state wave functions and eigenvalues are obtained from the DFT/PBE with norm-conserving pseudopotentials³². The plane-wave basis is set with a cutoff energy

of 60 Ry with a $8 \times 8 \times 1$ k -point grid. A vacuum space between neighboring layers is set to be more than 25 Å to avoid the interactions between layers. Based on these parameters, our calculated lattice constant **a** is 6.43 (6.78) Å and the lattice constant **b** is 6.53 (6.66) Å for ReS₂ and ReSe₂, respectively. They are consistent with previous calculations^{18,20}.

The quasiparticle energies and band gaps are calculated by the GW approximation within the general plasmon pole (GPP) model³³. The involved unoccupied conduction band number for calculating the dielectric function and self-energy is about ten times of the occupied valence band number. In solving the BSE, we use a finer k -point grid of $32 \times 32 \times 1$ for converged excitonic states³⁴. All the GW-BSE calculations are performed with the BerkeleyGW code³⁵ including the slab coulomb truncation scheme to mimic suspended monolayer structures^{36,37}. For optical absorption spectra, only the incident light polarized parallel with the plane is considered due to the depolarization effect^{38,39}.

III. QUASIPARTICLE ENERGIES AND BAND GAP

The DFT calculated band structures of monolayer ReS₂ and ReSe₂ are presented in Fig. 2. That with spin-orbit coupling (SOC) included is presented in the appendix. As shown in Fig. 2(a), monolayer ReS₂ exhibits a 1.36 eV direct band gap at the Γ point. This is consistent with a recent work¹⁸ reporting a value of 1.43 eV. On the other hand, at the DFT level, monolayer ReSe₂ is observed to be an indirect-gap semiconductor; the conduction band minimum (CBM) is located at the Γ point while the valence band maximum (VBM) is slightly away from the Γ point, as shown in Fig. 2(b) and its inset. The DFT-calculated indirect band gap of monolayer ReSe₂ is about 1.22 eV and the direct gap at the Γ point is slightly larger, about 1.25 eV. These are also consistent with previous DFT calculations^{19,20,25}.

However, it is well known that DFT usually underestimates the band gap of semiconductors. Therefore, we have performed the GW calculation to obtain reliable quasiparticle band gaps of monolayer ReS₂ and ReSe₂. Similar to those found in other monolayer 2D semiconductors, such as monolayer hexagonal TMDCs (MoS₂)⁷⁻¹⁰ and phosphorene⁴⁰, significant self-energy enhancements are observed in ReX₂; at the "single-shot" G_0W_0 level, the quasiparticle band gap of monolayer ReS₂ is increased to be 2.38 eV and that of monolayer ReSe₂ is increased to 2.09 eV, as listed in Table I. These enhanced many-electron effects are from

the depressed screening and reduced dimensionality of suspended 2D semiconductors^{7,9,40,42}.

Interestingly, the self-energy not only enlarges the band gap value but also may modify the band topology of ReX_2 . This is particularly significant for monolayer ReSe_2 , which is an indirect-gap semiconductor at the DFT level, as shown in Fig. 2(b). However, e - e interactions lower the valence band energy at the Λ point by about 50 meV more, compared to that of the Γ point. Therefore, the VBM is shifted to the Γ point, making monolayer ReSe_2 a direct-gap semiconductor, as listed in the blue-colored VBM in table II. However, it has to be pointed out that the indirect to direct transition may not be very sharp because the energy difference at the Γ/Λ point are very small and external perturbations may change the conclusion. On the other hand, it shall be true that the many-electron self-energy will increase the valence band energy at the Λ point and, at least, make the top of valence band almost degenerated. This will affect photoluminescence (PL) experiments.

These different self-energy corrections are resulted from the nature of the involved electronic states at the Γ and Λ points. For example, a major contribution to the self-energy is from the screened-exchange interaction (Σ_{SEX})³³, which is strongly affected by the spatial localization of electronic states. This can be seen from its static form³³:

$$\Sigma_{SEX}(r, r') = -\Sigma_{nk}^{occ} \phi_{nk}(r) \phi_{nk}^*(r') W(r, r'), \quad (1)$$

where the subscripts n is the band index and k is the sampling points in the reciprocal space, ϕ_{nk} is the electronic wave function, and W is the screened Coulomb interaction. Obviously, a smaller distance between r and r' enhances the overlap between wave functions and screened Coulomb interactions, giving rise to a larger self-energy. This non-uniform self-energy correction is similar to what have been observed in hexagonal TMDCs, i.e., the different self-energy corrections at the K point and the zone center of monolayer MoS_2 ⁹. Following this idea, we have checked the projected density of states (PDOS) of electronic states at the Γ and Λ points of ReSe_2 , as listed in Table II. The Λ_v valence state has more localized d -electron component (86%) than that the Γ_v valence state (78%). As a result, quasiparticle energy of the Λ_v state is enhanced more, meaning its energy level is lowered more and resulting in a switch of the VBM.

This direct quasiparticle band gap is not conflicted with experimental measurements, in which rather weak PL peak intensity is observed in monolayer ReSe_2 and the PL peak of ReSe_2 increases monotonically with increasing the layer number⁴³. This measurement seems

to hint an indirect-gap of ReSe₂. However, different from our calculated suspended and neutral cases, these measured samples are on substrates and are inevitably doped. Thus their self-energy corrections will be substantially reduced under these conditions, as shown in WSe₂ and MoS₂^{28,44}, meaning their measured samples may have a slightly indirect band gap. It has to be pointed out that this small energy difference is within the intrinsic error bars of DFT and GW methods. Thus more accurate experiments of suspended samples are important for conclusive results.

Finally, previous works have shown that the self-consistent GW (sc-GW) scheme beyond single-shot calculations may be necessary for 2D semiconductors^{9,40,42}. Therefore, we perform one self-consistent update to the Green's function G ; the quasiparticle band gap is further increased to 2.82 eV for monolayer ReS₂ and 2.45 eV for monolayer ReSe₂, as listed in Table I. Similar to monolayer MoS₂ and black phosphorus, we find that more self-consistent steps only slightly change the band gap ($\sim 0.1\text{eV}$) and we stop at the sc-G₁W₀ level. Finally, the SOC is significant in ReX₂ structures (around 150 meV of lowering the band gap)¹⁸. Considering all these factors, we compute the quasiparticle band gaps and summarize them in the last column of Table I. In the following, all our discussions and the BSE calculations are based on the finalized sc-G₁W₀ results with SOC included.

IV. EXCITON EFFECTS ON OPTICAL ABSORPTION SPECTRA

Because optical spectra of ReX₂ are anisotropic, we first focus on those with the incident light polarized along the Γ -K2 (x) directions because the corresponding optical absorption spectra can exhibit most features. Those of other polarizations will be discussed in Section V. First, the single-particle optical absorption spectra for monolayer ReS₂ and ReSe₂ are presented in Figs. 3(a) and (c) (blue dashed lines). As expected, the main optical absorption shoulder starts from the quasiparticle band gap, which are around 2.7 eV and 2.3 eV, for ReS₂ and ReSe₂, respectively.

Since e - h interactions are known to be crucial for obtaining reliable optical spectra in 2D semiconductors, we have solved the BSE to include them and present the optical absorption spectra in Fig. 3 by red solid lines. Similar to other 2D semiconductors, all main optical features are dominated by excitonic states in monolayer ReX₂. For example, after including e - h interactions, the first absorption peak of ReS₂ is located at 1.63 eV as shown in Fig. 3(a),

which is a strongly bound exciton with a 1.07-eV e - h binding energy. Monolayer ReSe₂ exhibits similarly enhanced excitonic effects as shown in Fig. 3(c) with the absorption peak at around 1.42 eV and exciton binding energy of 0.87 eV.

It has to be pointed out that the lowest-energy peak (1.42 eV) in the optical absorption spectrum of monolayer ReSe₂ is actually composed of two bright excitons (E_Γ and E_Λ), as elucidated in the insert of Fig. 3(c). The energy spacing of these two excitons is only about 96 meV. These two nearly degenerated excitons are resulted from the indirect-gap nature of ReSe₂. To see this, we have plotted the distributions of these exciton amplitudes in the reciprocal space (see details in Ref. 9). As shown in Fig. 4, the exciton E_Γ is mainly from the transitions around the zone center (the Γ point), while the exciton E_Λ is mainly from those around the Λ points. Since the energies of maxima of the valence band at the Γ and Λ points are very close to each other, the formed excitons obviously have very similar energies as well.

Recently, several PL measurements of monolayer ReS₂ and ReSe₂ have been performed. The measured broad PL peak position is about 1.50 to 1.65 eV at room temperature for ReS₂^{18,23} and 1.47 eV for ReSe₂²⁵. These experimental observations are in excellent agreement with our first-principles calculations, which we calculate as 1.6 eV and 1.4 eV for ReS₂ and ReSe₂, respectively. As shown in many previous works^{26–28}, the quasiparticle self-energy and e - h interactions partially cancel each other, making the final “optical” gap not much larger than the DFT-calculated band gap.

Finally, we have to address that Coulomb truncation is crucial for all above calculations^{27,29}. Without Coulomb truncation, both self-energy corrections and excitonic effects will be reduced because the actual simulation object is periodic structures with a large interlayer distance. For instance, for monolayer black phosphorus⁴⁰, the GW calculation with Coulomb truncation gives the band gap as 2 eV while that without truncation gives the value of 1.7 eV.

V. ANISOTROPIC EXCITON

Unlike hexagonal TMDCs, monolayer ReS₂ and ReSe₂ are the distorted 1-T diamond-chain with the triclinic symmetry. As a result, the optical absorption may be also anisotropic. This has been previously examined at the DFT level⁴⁵, where it is determined that the ab-

sorption spectra are anisotropic with respect to the polarization direction of the incident light. However, due to the incorrect band gaps and the short of e - h interactions, those DFT-calculations cannot be directly compared with experiments for providing reliable understanding. This motivates us to study the anisotropic optical responses at the level of including quasiparticle energy and excitonic effects.

Let us first focus on the case of monolayer ReS_2 . Its symmetry-induced anisotropic optical response can be seen even at the single-particle optical absorption level. As shown in Figs. 3(a) and (b), the single-particle optical absorption spectrum begins at near 2.7 eV for the incident light polarized along the Γ -K2 (x) direction, while it becomes significant at 2.9 eV for the light polarized along the Γ -M3 (y) direction. Previous studies have discussed this optical anisotropy^{45,46} and it is attributed to the transitions from non-bonding Re $5d$ t_{2g} to $5d$ t_{2g}^* and to anti-bonding chalcogen p and σ states⁴⁵. In Table II, we have listed the PDOS of band-edge states of monolayer ReS_2 and ReSe_2 . It is clear that both valence and conduction band edges are mainly made of Re $5d$ states and chalcogen p states. For example, the Γ_v state of ReS_2 has 11 percents of p state of S atoms and 80 percents of d state of Re atoms. This is consistent with previous studies⁴⁷.

The inclusion of e - h interactions does not essentially change the anisotropic optical response. As shown by red solid lines in Figs. 3(a) and (b), excitonic effects only lower the absorption edge but keep the anisotropy. For example, the lowest-energy excitonic peak of monolayer ReS_2 is at 1.63 eV for the incident light polarized along the Γ -K2 (x) direction and the absorption edge is located at 1.9 eV for the incident light polarized along the Γ -M3 (y) direction. Thus monolayer ReS_2 may work as an optical polarizer covering the frequency range from 1.6 eV to 1.9 eV, which is very interesting for near-infrared applications.

In order to have a complete picture of anisotropies of these important bright excitons, we present their optical oscillator strength with respect to the polarization angle of the incident light in Fig. 5. As expected, the optical oscillator strength of the prominent exciton of monolayer ReS_2 exhibits a figure-8 shape (Fig. 5(a)), which represents the spatial anisotropic optical response. For different directions, the optical oscillator strength can differ by two orders of magnitude. For instance, the intensity along Γ -K2 (x) direction is about 800 times stronger than that along Γ -M3 (y) direction. This anisotropic response can easily be observed by both optical absorption and PL experiments.

Monolayer ReSe_2 exhibits a similar anisotropic optical response, with some subtle differ-

ences. As shown in Figs. 3(c) and (d), the optical absorption spectra of monolayer ReSe₂ are different with respect to the polarization direction of incident light. However, the lowest-energy absorption peak (around 1.4 eV) along the Γ -K2 (x) direction does not completely disappear for the incident light polarized along the Γ -M3 (y) direction. This is different from the case of ReS₂. This complication arises from the fact that the lowest-energy peak of ReSe₂ actually consists of two excitons (E_Γ and E_Λ), instead of one in ReS₂, as shown in the insert of Figs. 3(c) and (d). E_Γ behaves similar to the lowest exciton in ReS₂, which is bright when the incident light is polarized along the Γ -K2 (x) direction, and dark along the Γ -M3 (y) direction. E_Λ , on the other hand, is not completely dark along the Γ -M3 (y) direction. Thus the lowest-energy peak does not have an extremely high polarization anisotropy.

This can be better understood by plotting the oscillator strength of the excitons E_Γ and E_Λ separately, which is shown in Figs. 5(b) and (c). Interestingly, both excitons, E_Γ and E_Λ , exhibit significant spatial anisotropy. However, the preferred direction of the exciton E_Λ is rotated by about 30 degrees. This is not surprising since the main contribution of the exciton E_Λ is from those states at the Λ points, which are not high-symmetry points. Finally, because the prominent absorption peak at 1.4 eV is the combination of these two excitons, it is obvious that the overall optical absorption does not show a complete anisotropy as shown in Fig. 5(d) with a 50-meV smearing. It has to be pointed out that PL experiments may exhibit stronger anisotropic optical spectra than the absorption measurements. At room temperature, the 96-meV gap between the excitons E_Γ and E_Λ will make most excited carriers collected by the lower-energy E_Γ exciton, resulting in a simpler anisotropic PL intensity similar to the exciton shown in Fig. 5(b).

VI. SUMMARY

In summary, first-principles GW-BSE simulations have been performed to study quasiparticle band gaps, excitonic effects, and optical spectra of distorted 1-T diamond-chain monolayer ReS₂ and ReSe₂. Monolayer ReS₂ is direct band gap semiconductor, and the quasiparticle band gap is 2.7 eV. Monolayer ReSe₂ changes from the DFT-calculated 1.22-eV indirect band gap to be a 2.3-eV direct one after GW corrections. Huge excitonic effects dominate optical spectra of suspended monolayer ReX₂, with around 1-eV e - h binding energies. The calculated absorption peaks are in excellent agreement with recent measurements.

Additionally, both the monolayer ReS_2 and ReSe_2 shows anisotropic optical responses due to their reduced triclinic symmetry lattices. In particular, the partially anisotropic optical absorption spectra of monolayer ReSe_2 are attributed to the two adjacent excitons, resulting from two nearby maxima at the valence band edge. Our calculations provide necessary information to clarify experimental measurements and our predictions are useful for broad near-infrared applications of distorted 1-T phase 2D semiconductors.

ACKNOWLEDGMENTS

We thank Vy Tran, Ruixiang Fei, and Han Wang for fruitful discussions. This work is supported by National Science Foundation Grant No. DMR-1207141. H.-X. Z. and J.-J. S. are supported by the National Basic Research Program of China (No. 2012CB619304) and the National Natural Science Foundation of China (No. 11474012). H.-X. Z. also acknowledges the financial support from the China Scholarship Council. The computational resources have been provided by the Lonestar of Teragrid at the Texas Advanced Computing Center (TACC).

-
- ¹ A. H. Castro Neto, F. Guinea, N. M. R. Peres, K. S. Novoselov, and A. K. Geim, *Rev. Mod. Phys.* **81**, 109 (2009).
 - ² Q. H. Wang, K. Kalantar-Zadeh, A. Kis, J. N. Coleman, and M. S. Strano, *Nat. Nanotechnol.* **7**, 699-712 (2012).
 - ³ A. Splendiani, L. Sun, Y. Zhang, T. Li, J. Kim, C.-Y. Chim, G. Galli, and F. Wang, *Nano. Lett.* **10**, 1271-1275 (2010).
 - ⁴ K. F. Mak, C. Lee, J. Hone, J. Shan, and T. F. Heinz, *Phys. Rev. Lett.* **105**, 136805 (2010).
 - ⁵ D. Xiao, G.-B. Liu, W. Feng, X. Xu, and W. Yao, *Phys. Rev. Lett.* **108**, 196802 (2012).
 - ⁶ T. Cao, G. Wang, W. Han, H. Ye, C. Zhu, J. Shi, Q. Niu, P. Tan, E. Wang, B. Liu, and J. Feng, *Nat. Comm.* **3**, 887 (2012).
 - ⁷ A. Ramasubramaniam, *Phys. Rev. B* **86**, 115409 (2012).
 - ⁸ H. Shi, H. Pan, Y.-W. Zhang, and B. I. Yakobson, *Phys. Rev. B* **87**, 155304 (2013).
 - ⁹ D. Y. Qiu, F. H. da Jornada, and S. G. Louie, *Phys. Rev. Lett.* **111**, 216805 (2013).

- ¹⁰ Y. Liang, S. Huang, R. Soklaski, and L. Yang, Appl. Rev. Lett. **103**, 042106 (2013).
- ¹¹ H. Liu, A. T. Neal, and P. D. Ye, ACS Nano **6**, 8563-8569 (2012).
- ¹² A. Geim and I. Grigorieva, Nature **499**, 419-425 (2013).
- ¹³ B. Radisavljevic, A. Radenovic, J. Brivio, V. Giacometti, and A. Kis, Nat. Nanotechnol. **6**, 147-150 (2011).
- ¹⁴ H.-J. Chuang, X. Tan, N. J. Ghimire, M. M. Perera, B. Chamlagain, M. M.-C. Cheng, J. Yan, D. Mandrus, D. Tomnek, and Z. Zhou, Nano lett. **14**, 3594-3601 (2014).
- ¹⁵ W. Liu, J. Kang, D. Sarkar, Y. Khatami, D. Jena, and K. Banerjee, Nano lett. **13**, 1983-1990 (2013).
- ¹⁶ S. Das, H.-Y. Chen, A. V. Penumatcha, and J. Appenzeller, Nano lett. **13**, 100-105 (2013).
- ¹⁷ Y. Zhang, T.-R. Chang, B. Zhou, Y.-T. Cui, H. Yan, Z. Liu, F. Schmitt, J. Lee, R. Moore, Y. Chen, et al., Nat. Nanotechnol. **9**, 111-115 (2014).
- ¹⁸ S. Tongay, H. Sahin, C. Ko, A. Luce, W. Fan, K. Liu, J. Zhou, Y.-S. Huang, C.-H. Ho, J. Yan, et al., Nat. Commun. **5**, 3252 (2014).
- ¹⁹ S. Yang, S. Tongay, Y. Li, Q. Yue, J.-B. Xia, S.-S. Li, J. Li, and S.-H. Wei, Nanoscale **6**, 7226-7231 (2014).
- ²⁰ D. Wolverson, S. Crampin, A. S. Kazemi, A. Ilie, and S. J. Bending, ACS Nano **8**, 11154-11164 (2014).
- ²¹ Z. Nan, J. Xiaoyu, G. Qiang, H. Yonghong, and M. Hui, Appl. Opt. **48**, 6734-6739 (2009).
- ²² E. Knill, R. Laflamme, and G. J. Milburn, Nature (London) **409**, 46-52 (2001).
- ²³ S. Horzum, D. Cakir, J. Suh, S. Tongay, Y.-S. Huang, C.-H. Ho, J. Wu, H. Sahin, and F. Peeters, Phys. Rev. B **89**, 155433 (2014).
- ²⁴ C. M. Corbet, C. McClellan, A. Rai, S. S. Sonde, E. Tutuc, and S. K. Banerjee, ACS Nano **9**, 363 (2014).
- ²⁵ S. Yang, C. Wang, H. Sahin, H. Chen, Y. Li, S.-S. Li, A. Suslu, F. M. Peeters, Q. Liu, J. Li, et al., Nano lett. **15**, 1660-1666 (2015).
- ²⁶ L. Wirtz, A. Marini, and A. Rubio, Phys. Rev. Lett. **96**, 126104 (2006).
- ²⁷ H.-P. Komsa and A.V. Krashenninnikov, Phys. Rev. B **86**, 241201(R) (2012).
- ²⁸ M.M. Ugeda, A.J. Bradley, S.-F. Shi, F.H. da Jornada, Y. Zhang, D.Y. Qiu, W. Ruan, S.-K. Mo, Z. Hussain, Z.-X. Shen, F. Wang, S.G. Louie, and M.F. Crommie, Nature Mater. **13**, 1091 (2014).

- ²⁹ A. Molina-Sánchez, D. Sangalli, K. Hummer, A. Marini, and L. Wirtz, *Phys. Rev. B* **88**, 045412 (2013).
- ³⁰ J. P. Perdew, K. Burke, and M. Ernzerhof, *Phys. Rev. Lett.* **77**, 3865 (1996).
- ³¹ P. Giannozzi, S. Baroni, N. Bonini, M. Calandra, R. Car, C. Cavazzoni, D. Ceresoli, G. L. Chiarotti, M. Cococcioni, I. Dabo, et al., *J. Phys.: Condens. Matter* **21**, 395502 (2009).
- ³² N. Troullier and J. L. Martins, *Phys. Rev. B* **43**, 1993 (1991).
- ³³ M. S. Hybertsen and S. G. Louie, *Phys. Rev. B* **34**, 5390 (1986).
- ³⁴ M. Rohlfing and S. G. Louie, *Phys. Rev. B* **62**, 4927 (2000).
- ³⁵ J. Deslippe, G. Samsonidze, D. A. Strubbe, M. Jain, M. L. Cohen, and S. G. Louie, *Comput. Phys. Commun.* **183**, 1269 (2012).
- ³⁶ S. Ismail-Beigi, *Phys. Rev. B* **73**, 233103 (2006).
- ³⁷ C. A. Rozzi, D. Varsano, A. Marini, E. K. Gross, and A. Rubio, *Phys. Rev. B* **73**, 205119 (2006).
- ³⁸ C. D. Spataru, S. Ismail-Beigi, L. X. Benedict, and S. G. Louie, *Appl. Phys. A: Mater. Sci. Process.* **78**, 1129-1136 (2004).
- ³⁹ L. Yang, C. D. Spataru, S. G. Louie, and M.-Y. Chou, *Phys. Rev. B* **75**, 201304 (2007).
- ⁴⁰ V. Tran, R. Soklaski, Y. Liang, and L. Yang, *Phys. Rev. B* **89**, 235319 (2014).
- ⁴¹ C. D. Spataru, S. Ismail-Beigi, L. X. Benedict, and S. G. Louie, *Phys. Rev. Lett.* **92**, 077402 (2004).
- ⁴² H. Shi, H. Pan, Y.-W. Zhang, and B. I. Yakobson, *Phys. Rev. B* **87**, 155304 (2013).
- ⁴³ H. Zhao, J. Wu, H. Zhong, Q. Guo, X. Wang, F. Xia, L. Yang, P.-H. Tan, and H. Wang, *arXiv:1504.07664* (2015).
- ⁴⁴ Y. Liang and L. Yang, *Phys. Rev. Lett.* **114**, 063001 (2015).
- ⁴⁵ C. Ho and C. Huang, *J. Alloys Compd.* **383**, 74-79 (2004).
- ⁴⁶ C. Ho, Y. Huang, and K. Tiong, *J. Alloys Compd.* **317**, 222-226 (2001).
- ⁴⁷ D. Çakir, H. Sahin, and F. M. Peeters, *Phys. Chem. Chem. Phys.* **16**, 16771 (2014).

TABLE I. DFT and GW band gaps (in unit of eV) for monolayer ReS₂ and ReSe₂.

	DFT	G ₀ W ₀	sc-G ₁ W ₀	sc-G ₁ W ₀ (SOC)
ReS ₂	1.36 1.43 ^a	2.38	2.82	2.69
ReSe ₂	1.22 1.24 ^b	2.09	2.45	2.29

^a Reference 18.

^b Reference 19.

TABLE II. The PDOS of the highest valence and lowest conduction band wave functions for monolayer ReS₂ and ReSe₂ at the k -points labelled in Fig. 2. The percent contributions from each atomic orbital for these wave functions are listed.

		Energy (eV)		Re			X	
		DFT	G ₀ W ₀	s	p	d	s	p
ReS ₂	Γ_v	0.00	0.00	0	5	80	3	11
	Γ_c	1.36	2.38	1	2	69	1	27
ReSe ₂	Γ_v	-0.02	0.02	0	6	78	0	16
	Γ_c	1.22	2.11	0	1	59	1	39
	Λ_v	0.00	0.00	0	4	86	0	10
	Λ_c	1.29	2.18	0	1	63	1	35

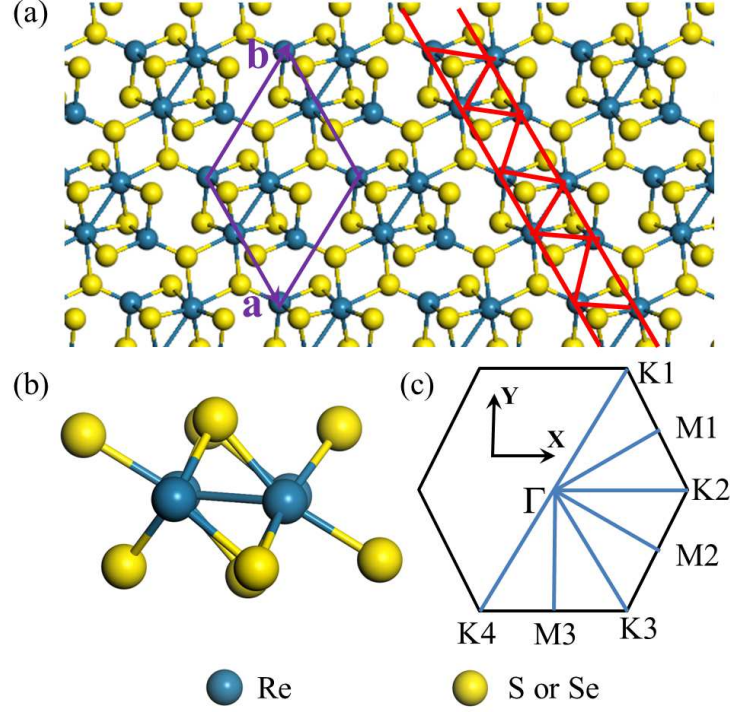


FIG. 1. (a) Top view of atomic structure of distorted 1-T diamond-chain monolayer ReX_2 . The clustering of Re atoms forms the zigzag chains along lattice vector \mathbf{a} direction, as shown in the red-line box. (b) The side view of monolayer ReX_2 . (c) The first Brillouin zone of monolayer ReX_2 .

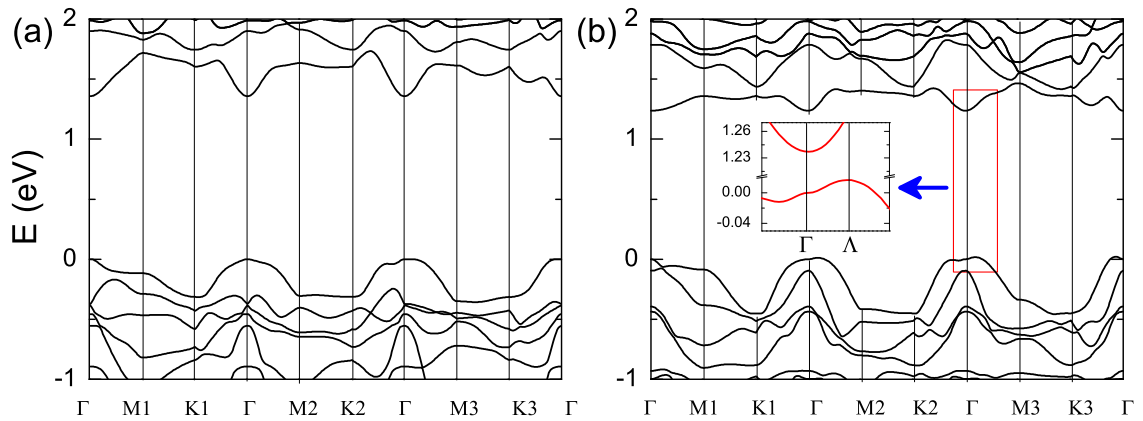


FIG. 2. The DFT-calculated band structures of monolayer ReS_2 (a), and ReSe_2 (b). The inset in (b) is the zoom of the band structure inside the red rectangle. The SOC is not included in these plots. The top of the valence band is set to be zero.

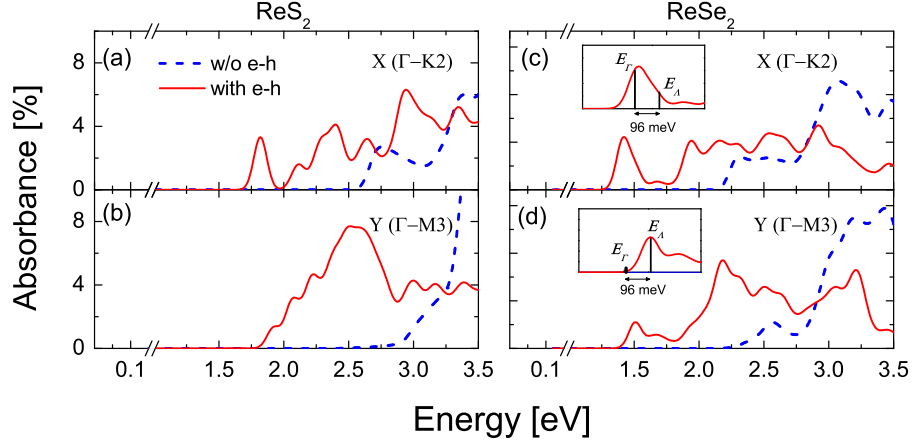


FIG. 3. Optical absorption spectra of monolayer ReS_2 (left) and ReSe_2 (right) for the incident light polarized along the Γ - K_2 direction ((a) and (c)) and the Γ - M_3 direction ((b) and (d)). The inset in (c) and (d) zoom in the lowest-energy absorption peaks, which is composed of two adjacent excitons (E_Γ and E_Λ) with an energy difference 96 meV in monolayer ReSe_2 . We employ 50 meV Gaussian smearing in these plots.

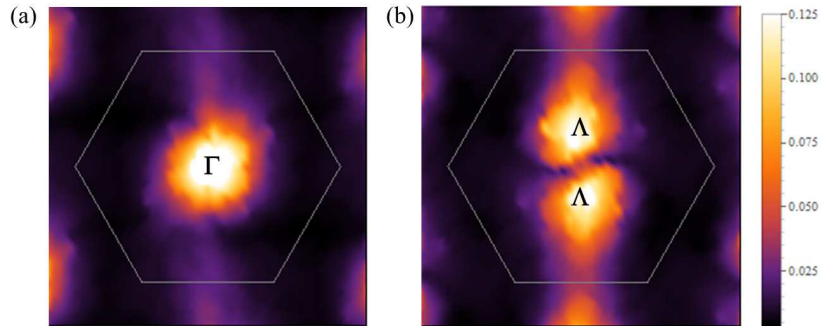


FIG. 4. The exciton amplitude distribution of the exciton E_Γ (a) and that of the E_Λ (b) (see Fig. 3) in monolayer ReSe_2 in reciprocal space.

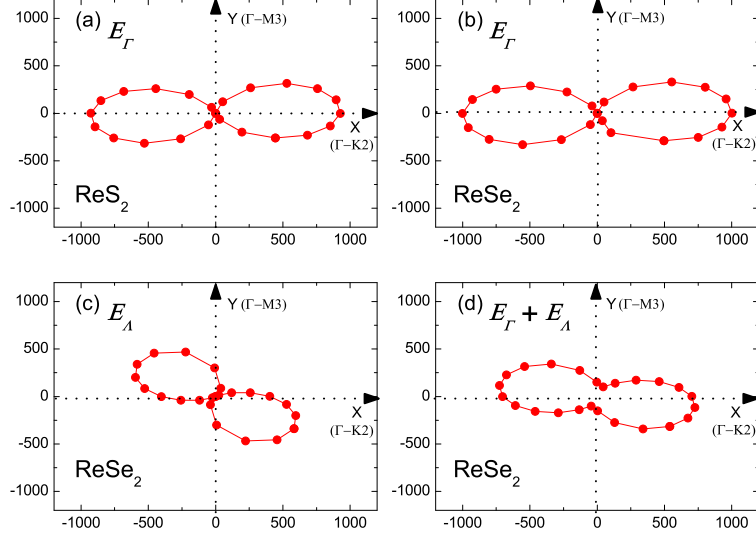


FIG. 5. Polarization-dependent oscillator strength (arbitrary unit) of excitons in monolayer ReSe₂ (a), the exciton E_Γ (b) and E_A (c) and their combined oscillator strength (d) in monolayer ReSe₂ with a 50-meV smearing to mimic the absorption spectrum.

Appendix: Band structure of monolayer ReX_2 with SOC included

Since Re atoms are heavy atomic species, we thus take into accounts of SOC in Fig. 6. Compared with the band structures in Fig. 2. the SOC slightly reduces the band gap of monolayer ReX_2 , which is also clearly presented in Table I.

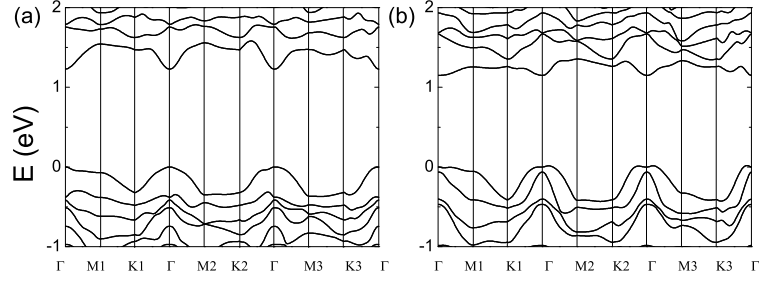


FIG. 6. The DFT-calculated band structures of monolayer ReS_2 (a), and ReSe_2 (b) with SOC included. The energy of the top of the valence band is set to be zero.